In-depth immunometabolic profiling by measuring single-cell protein translation inhibition via bioorthogonal noncanonical amino acid tagging (SCENITH-BONCAT)

Frank Vrieling[1], Hendrik J.P. van der Zande[1], Lisa Smeehuijzen[1], Jan van den Bossche[2], Sander Kersten[1], Rinke Stienstra[1,3]

1. Division of Human Nutrition and Health, Wageningen University, Wageningen, The Netherlands

2. Department of Molecular Cell Biology and Immunology, Amsterdam Cardiovascular Sciences, Amsterdam Gastroenterology Endocrinology Metabolism, Amsterdam Institute for Infection and Immunity, Cancer Centre Amsterdam, Amsterdam UMC, Vrije Universiteit Amsterdam, Amsterdam, the Netherlands

3. Department of Internal Medicine, RadboudUMC, Nijmegen, The Netherlands

Corresponding author:

Rinke Stienstra

Email: rinke.stienstra@wur.nl

34 Keywords: Immunometabolism, SCENITH, energy metabolism, glycolysis, OXPHOS

Abstract:

Motivation:

Seahorse Extracellular Flux (XF) analysis has been influential in immunometabolism research, measuring cellular oxygen consumption rate (OCR) and extracellular acidification rate (ECAR) to determine immune cell metabolic profiles. However, Seahorse XF has several limitations, relying on purified adherent cells, relatively high cell numbers, and specialized equipment and reagents. Recently, a novel flow cytometry-based technique called SCENITH (Single Cell Energetic metabolism by profiling Translation inhibition) was introduced, which measures cellular protein synthesis through puromycin staining as a proxy for metabolic activity in single cells. The current limitation of SCENITH is its reliance on a specific anti-puromycin antibody that is not commercially available. To address this, we propose an alternative approach using biorthogonal noncanonical amino acid tagging (BONCAT) to measure protein synthesis.

Summary:

The field of immunometabolism has revealed that cellular energy metabolism significantly contributes to immune cell function. Disturbances in immune cell metabolism have been associated with various diseases, including obesity, atherosclerosis, and cancer. To further advance immunometabolic research, developing novel methods to study the metabolism of immune cells in complex samples is required. Here, we introduce SCENITH-BONCAT, an adapted version of SCENITH which utilizes click-labeling of homopropargylglycine (HPG), an alkyne-bearing methionine analog, to measure protein synthesis as a proxy of metabolic activity. SCENITH-BONCAT successfully reproduced known metabolic signatures of immune cell activation. Specifically, LPS/IFNγ-induced classical activation increased glycolytic capacity, and IL-4-induced alternative activation enhanced mitochondrial dependence in human macrophages. The assay's applicability was further explored in peripheral blood mononuclear cells (PBMCs) from healthy volunteers, revealing diverse metabolic rewiring in immune cell subsets upon stimulation with different activators. Cryopreserved PBMCs showed reduced HPG incorporation and mitochondrial dependence compared to freshly isolated cells, warranting attention to cellular mitochondrial health during cryopreservation. Finally, SCENITH-BONCAT was used to analyze murine tissue-resident immune cells from different organs. Principal component analysis (PCA) revealed tissue-specific clustering based on metabolic profiles, likely driven by microenvironmental priming of tissue-resident immune cells. In conclusion, SCENITH-BONCAT offers valuable insights into immune cell metabolic responses and presents a powerful platform for studying immune cell metabolism in complex samples and tissue-resident immune populations in both human and murine studies.

68 **Introduction:**

69 The expanding field of immunometabolism has demonstrated that the functional properties of immune
70 cells are dependent on how these immune cells produce energy, i.e., by their metabolic profile. When
71 immune cells are activated, their energy demand increases to support proliferation and effector functions
72 such as the production of cytokines and antibodies. This process involves a significant reprogramming of
73 cellular metabolic pathways. Upon activation, many immune cell types switch from oxidative
74 mitochondrial metabolism to glycolysis, a phenomenon known as the 'Warburg effect' as it was first
75 described in tumor cells by Otto Warburg (Warburg et al., 1927). Although essential for immune
76 function, alterations in immune cell metabolism have been associated with various pathologies. For
77 example, chronic low-grade inflammation in adipose tissue is linked to metabolic rewiring of adipose
78 tissue macrophages in obesity (Boutens et al., 2018), while 'primed' glycolytic inflammatory monocytes
79 are associated with atherosclerosis (Shirai et al., 2016). In tumors, immune cell metabolism is
80 reprogrammed by limitations in nutrient availability and the accumulation of metabolic byproducts such
81 as lactate, hindering their effector functions (Kaymak et al., 2021). Hence, technologies that enable
82 detailed analysis of cellular metabolism are essential for studying the underlying mechanisms of
83 inflammatory diseases.

84 Seahorse Extracellular Flux (XF) analysis has been instrumental in making many discoveries in the
85 immunometabolism field. This technique measures cellular oxygen consumption rate (OCR) and
86 extracellular acidification rate (ECAR) to determine functional metabolic profiles. However, this method
87 has limitations, including its reliance on purified, adherent cells, relatively high cell numbers, and
88 specialized equipment and reagents. With the advent of single-cell technologies, developing novel
89 methods to determine functional metabolic profiles of immune cells in complex samples is of great
90 importance. A paper by Argüello et al. recently introduced a technique called SCENITH (Single Cell
91 Energetic metabolism by profiling Translation inhibition). The core principle of SCENITH is that the rate of
92 cellular protein synthesis reflects metabolic activity and can be used to determine cellular metabolic
93 dependencies. In SCENITH, the incorporation of the antibiotic puromycin into nascent proteins is
94 measured through immunostaining as a proxy for protein synthesis under conditions of metabolic
95 inhibition (2-deoxy-D-glucose to inhibit glucose metabolism, oligomycin to inhibit mitochondrial ATP
96 synthesis), allowing for the determination of cellular dependence on glucose and mitochondrial
97 metabolism. Since SCENITH is a flow cytometry-based assay, it offers single-cell resolution and requires
98 significantly fewer cells than Seahorse XF analysis. This method has been compared and validated
99 against Seahorse XF analysis (Argüello et al., 2020; Verberk et al., 2022) and is thus a promising tool for
100 determining functional metabolic profiles of immune cells in complex samples.

101 A significant limitation of SCENITH in its current form is its reliance on a specific anti-puromycin antibody
102 (clone R4743L-E8), which is not commercially available. Therefore, we propose an alternative way of
103 measuring protein synthesis in SCENITH through biorthogonal noncanonical amino acid tagging
104 (BONCAT) (Dieterich et al., 2006). During BONCAT, the amino acid methionine is replaced with a non-
105 natural analog containing a minimal modification, either the azide-bearing azidohomoalanine (AHA) or
106 the alkyne-bearing homopropargylglycine (HPG). After incubation of cells with the amino acid, nascent
107 proteins containing AHA or HPG can be fluorescently tagged through copper(I)-catalyzed azide-alkyne
108 cycloaddition (CuAAC) (Beatty et al., 2005), which is commonly known as a 'click' reaction. Among
109 others, BONCAT has been used for affinity purification of nascent proteins (Landgraf et al., 2015), to
110 track and localize the newly synthesized proteins in cells (Shen et al., 2021), and to measure SLC1A5-
111 mediated amino acid uptake (Pelgrom et al., 2022). A significant advantage of using BONCAT to measure
112 protein synthesis over anti-puromycin immunostaining is increased flow cytometry panel design flexibility
113 due to access to various fluorescent click probes. Moreover, AHA and HPG are non-toxic compared to
114 puromycin (Su Hui Teo et al., 2016), which can induce ER stress (Oguma et al., 2009) and other toxic
115 effects (Aviner, 2020).

116 Here, we applied SCENITH-BONCAT using HPG in a 'one size fits all' format for measuring metabolic
117 dependencies in multiple sample types (Figure 1). We show that cells incorporate HPG over time due to
118 protein synthesis and validate our method compared to the original SCENITH protocol in a primary

119 macrophage model of classical versus alternative activation. Next, we tested the application of SCENITH-
120 BONCAT for metabolic profiling of peripheral blood mononuclear cells (PBMCs) under different stimulatory
121 conditions. Finally, we demonstrate the technique's effectiveness in analyzing tissue-resident immune
122 cell metabolism in mice.

123 **Materials & Methods:**

124 *Reagents, culture media, and supplements*

125 L-homopropargylglycine (HPG), THPTA, AZDye 405 Azide Plus, and AZDye 488 Azide Plus were bought
126 from Click Chemistry Tools. Lipopolysaccharide from *Escherichia coli* O55:B5 (LPS), oligomycin, 2-deoxy-
127 D-glucose (2-DG), L-Cystine dihydrochloride, RPMI 1640 medium (with sodium bicarbonate, without
128 methionine, cystine and L-glutamine) and homoharringtonine were purchased from Merck. Fetal calf
129 serum (FCS) was acquired from Biowest. RPMI 1640 medium (with sodium bicarbonate, without L-
130 glutamine and HEPES), GlutaMAX™, and dialyzed FCS were bought from Thermo Fisher. Interferon γ
131 (IFNγ) and interleukin 4 (IL-4) were acquired from Peprotech. ODN2006 was purchased from HyCult.
132 TransAct was bought from Miltenyi Biotec. Penicillin-Streptomycin Solution was obtained from Corning.

133

134 *Flow cytometry antibodies and reagents*

135 Anti-human antibodies: CD4-BV605, CD8-BV650, CD14-APC, CD16-PerCP-Cy5.5, CD19-PE-Dazzle594,
136 CD45RA-BV785, CD62L-BV405 and HLA-DR-PE-Cy7 were bought from Biolegend. CD56-PE was
137 purchased from Beckman Coulter.

138 Anti-mouse antibodies: B220-Alexa Fluor 700, CD3-Alexa Fluor 700, CD11b-BV650, CD11c-BV605,
139 CD45-APC-Fire750, CD45-PE-Dazzle594, CD64-PE, CLEC2-FITC, F4/80-FITC, Ly6C-APC, Ly6G-PerCP-
140 Cy5.5, MHCII-BV785, NK1.1-Alexa Fluor 700, Siglec-F-PE-Cy7, TIM4-PE, were acquired from Biolegend.

141 Zombie Aqua Fixable Viability Dye and Human TruStain FcX Fc Receptor Blocking Solution were from
142 BioLegend. CF700-SE and CF750-SE were bought from Biotium. Brilliant Stain Buffer Plus (BD
143 Biosciences was added to antibody mixes to prevent staining artifacts caused by interactions between
144 Brilliant Violet dyes. In mouse experiments, True-Stain Monocyte Blocker (Biolegend) was used to avoid
145 non-specific antibody binding of PE- and APC-based tandem dyes by myeloid cells.

146

147 *Peripheral blood mononuclear cell (PBMC) isolation and stimulation*

148 EDTA blood was collected from healthy volunteers after acquiring informed consent as per the norms of
149 the International Declaration of Helsinki. Blood tubes were pooled and diluted 1:1 in PBS, after which
150 PBMCs were isolated by Ficoll Paque Plus (Merck) gradient centrifugation in Leucosep™ tubes (Greiner
151 Bio-One). PBMC layers were collected in a 50 ml tube and washed thrice with PBS before counting using
152 a hemocytometer. PBMCs were resuspended at a density of 10×10^6 cells/mL in RPMI 1640 medium
153 supplemented with 10% FCS, GlutaMAX, and P/S and cultured in FACS tubes at 37°C/5%CO_2 while
154 shaking (100 RPM). To activate PBMCs, cells were stimulated with LPS (100 ng/mL), ODN 2006 (1 μM),
155 TransAct (1:100), or a mixture of all three stimuli for 1 hour before methionine depletion.

156

157 *Human monocyte isolation and macrophage differentiation*

158 Human primary monocytes were isolated from buffy coats of healthy blood bank donors through
159 magnetic-activated cell sorting (MACS). After PBMC isolation as described above, $CD14^+$ monocytes were
160 magnetically labeled using MojoSort Human CD14 Nanobeads (Biolegend) and subsequently separated
161 on LS columns using a QuadroMACS™ Separator (Miltenyi Biotec BV). Isolated monocytes were counted
162 using a Vi-CELL XR Cell Analyzer (Beckman Coulter), resuspended at a density of 1×10^6 cells/mL in RPMI
163 1640 medium supplemented with 10% FCS, GlutaMAX and P/S, and seeded in T75 flasks using 10 mL
164 per flask (10×10^6 cells). Monocytes were cultured for six days at 37°C/5%CO_2 in the presence of either
165 M-CSF (50 ng/mL; Miltenyi) or GM-CSF (5 ng/mL; Miltenyi) for macrophage differentiation. At day 3 of
166 differentiation, 5 mL of fresh medium containing M-CSF or GM-CSF was added to each flask.

After differentiation, macrophages were harvested by trypsinization and seeded in 24-well plates at a density of 3×10^5 cells/well (GM-CSF) or 4×10^5 cells/well (M-CSF). Macrophages were subsequently left untreated, classically activated by a combination of LPS (100 ng/mL) and IFNγ (10 ng/mL), or alternatively activated using IL-4 (20 ng/mL) for 24 hours.

Mice experiments

All experiments followed the Guide for the Care and Use of Laboratory Animals of the Institute for Laboratory Animal Research and were approved by the Central Authority for Scientific Procedures on Animals (CCD, AVD10400202115283) and the Institutional Animal Care and Use Committee of Wageningen University. Naïve, 12-week-old, male wild-type C57BL/6J mice were sacrificed by cervical dislocation, and epidydimal white adipose tissue (eWAT) fat pads, kidneys, liver, lungs, and spleen were collected in RPMI for tissue-resident immune cell isolation. Before collecting tissues, the peritoneal cavity was washed with 10 mL ice-cold PBS supplemented with 2 mM EDTA to isolate peritoneal exudate cells (PECs). Tissue-resident immune cells were isolated as described previously (Liu et al., 2020; vanderZande et al., 2023) with minor adaptations. Briefly, eWAT, kidneys, liver, and lungs were cut into small pieces using razors, and the spleen was mechanically disrupted using a syringe plunger. eWAT fat pads were digested in 5 mL digestion buffer containing 1 mg/mL collagenase type II from *Clostridium histolyticum* (Sigma-Aldrich) in Krebs buffer supplemented with 100 mM HEPES, 20 mg/mL BSA and 6 mM D-Glucose for 45 minutes at 37°C/5%CO_2 while shaking (100 RPM). Digestion was stopped by adding 5 mL wash buffer (PBS supplemented with 1% FCS and 2.5 mM EDTA), and the solution was filtered through 250 µm Nitex filters (Sefar). Infranatant containing SVF was collected, and erythrocytes were lysed using ice-cold erythrocyte lysis buffer (in-house, 0.15 M NH_4Cl, 1 mM $KHCO_3$, 0.1 mM Na_2EDTA). Cells were finally filtered through 40 µm cell strainers (PluriSelect).

Kidneys and lungs were digested in 5 mL digestion buffer containing 1 mg/mL collagenase V, 1 mg/mL dispase II, and 30 U/mL DNase I in RPMI for 30 minutes at 37°C/5%CO_2 while shaking (100 RPM). Digestion was stopped by adding 5 mL wash buffer, and the digest was filtered through 100 µm cell strainers (PluriSelect). After erythrocyte lysis and filtering through 40 µm cell strainers, kidney leukocytes were purified using magnetic-assisted cell sorting (MACS) using CD45 microbeads (35 µl per sample, Miltenyi Biotec) according to manufacturer's instructions.

The liver was digested in 5 mL RPMI supplemented with 1 mg/mL collagenase V, 1 mg/mL dispase II, 1 mg/mL collagenase D and 30 U/mL DNase I for 25 minutes at 37°C/5%CO_2 while shaking (100 RPM). Digest was filtered through 100 µm cell strainers and washed twice with 40 mL wash buffer (300 RCF, 5 minutes, 4°C). After erythrocyte lysis and filtering through 40 µm cell strainers, leukocytes were isolated using CD45 MACS, as was the case for the kidneys.

The spleen was digested in 5 mL digestion buffer containing 1 mg/mL collagenase D and 30 U/mL DNase I in RPMI for 30 minutes at 37°C/5%CO_2 while shaking (100 RPM). Digest was filtered through 100 µm filters, incubated with erythrocyte lysis buffer, and filtered again through 40 µm filters.

All isolated and filtered cells were counted using a hemocytometer, and $2.5\text{x}10^5$ eWAT, kidney, and peritoneal leukocytes/well, $5\text{x}10^5$ liver and lung leukocytes/well, and $1\text{x}10^6$ splenocytes/well were plated in 96-well U-bottom plates for SCENITH-BONCAT.

SCENITH-BONCAT

Methionine depletion and inhibitor treatment

Cells (human PBMCs, human primary macrophages, or mouse tissue-resident immune cells) were cultured for 30-45 minutes at 37°C/5%CO_2 in methionine-free RPMI 1640 supplemented with 65 mg/L L-cystine dihydrochloride, 10% dialyzed FCS, GlutaMAX and P/S to deplete intracellular methionine levels. Any ongoing stimulation (*e.g.* LPS, ODN 2006, TransAct) was refreshed in this medium. Cells were then

214 pre-incubated with metabolic inhibitors (10× work stocks in complete methionine-free RPMI) for 15
215 minutes to ensure complete shutdown of glucose and/or mitochondrial metabolism. The following four
216 treatments were applied in duplicate per experimental condition: DMSO (control), 2-deoxyglucose (2-
217 DG; 100 mM), oligomycin (1 μM), and a combination of 2-DG and oligomycin. All treatments were
218 corrected for DMSO and H_2O content. Cells were subsequently treated with HPG (100 μM) and incubated
219 for 30 minutes at 37°C/5%CO_2. After HPG incorporation, macrophage samples were washed 1× with
220 PBS, harvested by scraping, and transferred to a V-bottom 96-well plate. PBMC samples and mouse
221 tissue-resident immune cells were transferred to a V-bottom 96-well plate and pelleted through
222 centrifugation at 500RCF for 3 minutes, after which the supernatant was discarded by firmly flicking the
223 plate once. Cells were then washed 1× with PBS.

224 HPG was added directly after methionine depletion with or without homoharringtonine (20 μg/mL) or
225 DMSO control for kinetic experiments. Macrophages were harvested at T = 0, 0.5, 1, 2, 4, and 6 hours
226 post-treatment.

227

228 *Fluorescent click labeling of HPG and flow cytometry*

229 Human cells were pelleted by centrifugation and incubated with Zombie Aqua Fixable Viability Dye
230 (1:1000 in PBS) for 5-10 minutes at RT in the dark. Cells were then pelleted by centrifugation and fixed
231 in 2% formaldehyde for 15 minutes at RT. After fixation, cells were pelleted and washed 1× with PBS
232 before permeabilization with 0.1% saponin in PBS/1%BSA for 15 minutes at RT. Next, cells were washed
233 1× with PBS and barcoded with amine-binding dyes (CF700-SE and CF750-SE), 1 mM stocks) for 5
234 minutes at RT. Barcoding dyes were applied in four combinations of two dilutions (1:1000 and
235 1:100,000), allowing for pooling the four treatment conditions per replicate. Cells were then washed 1×
236 with PBS, and barcoded samples were pooled in Click buffer (100 mM Tris-HCl, pH 7.4). HPG was labeled
237 through copper(I)-catalyzed azide-alkyne cycloaddition (CuAAC) using the following reaction mix in Click
238 Buffer: 0.5 mM Cu(II)SO_4, 10 mM sodium ascorbate, 2 mM THPTA and 0.5 μM AF488 Azide Plus. Freshly
239 prepared sodium ascorbate solution (100 mM stock) and AZDye 488 Azide Plus were added to the
240 mixture just before addition to the samples. Click reaction was performed for 30 minutes at RT, after
241 which the cells were washed 2× with FACS buffer (PBS/1%BSA + 2 mM EDTA). PBMC samples were then
242 blocked with Human TruStain FcX Fc Receptor Blocking Solution (1:100) before staining with fluorescent
243 antibodies for 15 minutes at RT in the presence of Brilliant Stain Buffer.

244 Mouse cells were processed similarly with minor adjustments. Mouse cells were barcoded before
245 permeabilization using anti-CD45 antibodies (PE-Dazzle594- and APC-Fire750-conjugated) at 1:200 or
246 1:800 dilution for 15 minutes at RT. In addition, 0.5 μM AF405 Azide Plus was used for CuAAC, and
247 mouse tissue-resident immune cells were stained with a fluorescent antibody cocktail in the presence of
248 Brilliant Stain Buffer and TrueStain Monocyte Blocker.

249 Cells were washed 1× with FACS buffer after staining and acquired on a CytoFLEX S cytometer (Beckman
250 Coulter).

251

252 *Flow cytometry and statistical analysis*

253 Human macrophage and murine tissue flow cytometry data were analyzed using FlowJo software version
254 10.8.1 (Becton Dickinson). Human PBMC flow cytometry data were analyzed using OMIQ software from
255 Dotmatics (www.omiq.ai, www.dotmatics.com).

256 Principal component analysis (PCA) was performed in R version 4.2.2 using the mixOmics package
257 version 6.23.4 (Le Cao et al., 2021). R plots were made using the following packages: ggplot2 version
258 3.4.22 (Wickham et al., 2023), cowplot version 1.1.1 (Wilke, 2020), and ggh4x 0.2.4 (van den Brand,
259 2023). Statistical significance was tested by Repeated One-Way ANOVA with Dunnett's multiple

comparisons test or Two-Way ANOVA with Sidak correction for multiple testing using GraphPad Prism software version 8.01.

262 **Results**

263 *SCENITH-BONCAT: assay concept*

264 The assay concept is depicted in Figure 1. After sample workup and plating (1), cells are cultured in
265 methionine-free medium for 1 hour to deplete intracellular methionine (2). Next, the cells are pre-
266 incubated with DMSO as control, 2-DG to inhibit glucose metabolism, oligomycin to inhibit mitochondrial
267 respiration, or the compounds in combination to block ATP production completely (3). The methionine
268 analog HPG is subsequently added as a substrate for protein synthesis (4). Cells are then fixed and
269 permeabilized, after which intracellular HPG can be labeled through a click reaction with a fluorescent
270 azide probe to be measured by flow cytometry (5). By comparing HPG mean fluorescence intensities
271 between the different inhibitor conditions, it is possible to calculate the relative cellular metabolic
272 dependence on glucose and mitochondrial respiration (6) (Argüello *et al.*, 2020).

273

274 *HPG incorporation is a proxy of protein synthesis and can be used as an alternative to puromycin*

275 HPG is an alkyne-bearing methionine analog (Figure 2A) previously used to tag nascent proteins
276 (Landgraf *et al.*, 2015). To validate whether HPG incorporation in immune cells reflects protein synthesis,
277 M-CSF differentiated primary human macrophages were treated with HPG for up to 6 hours in the
278 presence or absence of homoharringtonine, a protein translation inhibitor. HPG accumulated in
279 macrophages over time as measured by flow cytometry (Figure 2B). This accumulation was entirely
280 blocked by treatment with homoharringtonine (Figure 2C), demonstrating that HPG incorporation can be
281 used as a proxy for protein synthesis.

282 Next, to test whether SCENITH-BONCAT could reproduce the results of the original SCENITH protocol
283 using the anti-puromycin antibody clone R4743L-E8, both assay variants were applied side-by-side to
284 analyze the metabolic profiles of primary human macrophages after classical activation (LPS + IFNγ)
285 versus alternative activation (IL-4). LPS activation in macrophages is associated with the upregulation of
286 glycolysis and a disrupted tricarboxylic acid (TCA) cycle, whereas IL-4 polarization is supported by
287 enhanced mitochondrial oxidative phosphorylation (OXPHOS) (Van den Bossche et al., 2017). As
288 expected, classical activation resulted in a relative increase in glycolytic capacity over mitochondrial
289 dependence. At the same time, the inverse was observed for alternative activation in both GM-CSF
290 (Figure 2D) and M-CSF (Figure 2E) differentiated macrophages. This result was obtained irrespective of
291 whether HPG or puromycin detection was used as a proxy for protein synthesis. Regarding glucose
292 dependence, both GM-CSF and M-CSF macrophages were highly glucose-dependent (>73%) across the
293 different polarized states, as evidenced by both techniques (Supplementary Figure 1). While polarization
294 did show some effects on glucose dependence using puromycin that was not recapitulated by HPG in GM-
295 CSF macrophages (Supplementary Figure 1A), the absolute values were not significantly different
296 between both techniques. These results establish SCENITH-BONCAT as a viable method for performing
297 immune cell metabolic profiling.

298

299 *SCENITH-BONCAT reveals differential metabolic responses to inflammatory stimulation in PBMCs*

300 An essential improvement of SCENITH over other techniques, such as Seahorse XF analysis, is its ability
301 to perform metabolic profiling of multiple cell types simultaneously in complex samples. Therefore, we
302 next tested the applicability of SCENITH-BONCAT to determine metabolic dependencies in PBMCs using a
303 nine-marker flow cytometry panel to identify B cells, monocytes, CD4 T cells, CD8 T cells, and NK cells
304 (Figure 3B). The gating strategy employed is illustrated in Supplementary Figure 2. We aimed to
305 investigate the metabolic profile of these cells in both their resting state and after immune cell activation.
306 A combination of immunological stimuli was applied to achieve this, as different immune cell types are
307 activated through distinct cell surface receptors. For instance, myeloid cells, such as monocytes, highly
308 express the TLR4 receptor, which recognizes LPS. B cells respond strongly to DNA containing
309 unmethylated CpG sequences via TLR9, whereas T cells are activated by co-activating the T cell co-

310 receptor CD3 and its co-stimulatory receptor CD28. Therefore, to determine the effect of immune
311 activation on metabolic dependencies, PBMCs were either left untreated (medium) or stimulated for 2
312 hours with LPS (TLR4 ligand), ODN2006 (CpG, TLR9 ligand), TransAct (synthetic CD3/CD28 agonist) or a
313 mixture containing all three ligands (Figure 3A).

314 HPG incorporation was differentially elevated by stimulation in all tested immune cells (Figure 3C). The
315 stimuli mixture (Mix) generally yielded similar results as the most potent single stimulation for each cell
316 type. As expected, B cells showed the highest HPG incorporation after treatment with the TLR9 ligand
317 ODN2006, while both CD4 and CD8 T cells most strongly responded to CD3/CD28 activation by TransAct.
318 $CD14^+/CD16^-$ classical monocytes showed a similar increase in HPG levels for all single stimulations.
319 Glucose dependence (Figure 3D) was very high (>90%) in classical monocytes, non-classical monocytes,
320 and B cells across all stimuli. Classical monocytes showed a substantial glycolytic shift in response to
321 stimulation (Figure 3E), with mitochondrial dependence decreasing from 66.1% to non-detectable levels
322 after LPS treatment. B cells similarly showed reduced mitochondrial dependence after activation with
323 ODN2006 and LPS, from 24.6% to 12.6% and 15.6%, respectively. $CD14^-/CD16^+$ non-classical
324 monocytes showed a very high mitochondrial dependence at baseline (95.0%) unaffected by stimulation,
325 although this monocyte subset could no longer be identified after LPS stimulation. CD4 and CD8 T cells
326 showed very low levels of HPG incorporation when untreated, indicating that these cell types are
327 relatively quiescent when inactive. As a result, small fluctuations in HPG signal could majorly skew the
328 relative metabolic dependencies in these cells, leading to highly variable and even negative values. In
329 line with the literature, activated T cells were highly glucose-dependent and relatively glycolytic. Within
330 the T cell subsets, $CD45RA^+$ T cells (Naïve & Effector) showed strongly increased HPG incorporation after
331 TransAct stimulation, whereas $CD45RA^-$ T cells (Central Memory & Effector Memory) also reacted to LPS
332 stimulation (Supplementary Figure 3). Similar to T cells, NK cells showed relatively low HPG
333 incorporation. NK cells responded most strongly to LPS stimulation of PBMCs, which increased their
334 glucose and mitochondrial dependence.

335 The above data show that SCENITH-BONCAT can be used to determine individual immune cell metabolic
336 profiles in PBMCs. During human studies, however, PBMCs are often cryopreserved directly after isolation
337 for later processing. To investigate whether cryopreservation is compatible with metabolic profiling using
338 SCENITH-BONCAT, PBMCs isolated from healthy volunteers were split into two fractions, one of which
339 was directly assayed after isolation (Fresh) while the other was cryopreserved at -80°C (Frozen) for up
340 to two weeks before measurements. Cryopreservation reduced immune cell HPG incorporation after
341 activation (Supplementary Figure 4A). Additionally, overall immune cell mitochondrial dependence
342 decreased after cryopreservation (Supplementary Figure 4B). This was especially evident for resting
343 classical monocytes, whose average mitochondrial dependence dropped from 75.3% in fresh samples to
344 16.4% after cryopreservation. Thus, caution should be exercised when performing SCENITH-BONCAT or
345 any other assay of metabolism on cryopreserved cells, as this process appears to deteriorate cellular
346 mitochondrial health (Acin-Perez et al., 2020).

347

348 *Metabolic profiling of murine tissue-resident immune cell populations*

349 After establishing the use of SCENITH-BONCAT for the metabolic profiling of complex samples, we next
350 tested its potential for analyzing tissue-resident immune cell populations in mice. Naïve, 12-week-old,
351 male wild-type C57BL/6J (n=6) were sacrificed, after which epididymal white adipose tissue (eWAT),
352 kidneys, livers, lungs, peritoneal exudate cells (PEC) and spleens were extracted. Upon tissue-resident
353 immune cell isolation, cells were subjected to SCENITH-BONCAT. A 9 marker flow cytometry was used
354 to identify conventional dendritic cell subsets (cDC1 and cDC2), tissue-specific macrophage populations,
355 monocytes, B cells, neutrophils, eosinophils, $Ly6C^-$ and $Ly6C^{hi}$ non-B lymphocytes. The complete gating
356 strategies are depicted in Supplementary Figure 5.

357 HPG incorporation levels were variable across tissues and cell types (Figure 4A). In general, tissue-
358 resident immune cells in PEC and spleen samples showed the highest HPG fluorescence intensities, while
359 HPG accumulation was relatively low in kidney and liver immune cells. This is most likely related to the

360 purity of the sample, as cells from PEC and spleen are almost solely of leukocytic origin, whereas kidney
361 and liver samples still contain other cell types and biological material which could interfere with HPG
362 uptake, even after $CD45^+$ magnetic cell sorting. Within tissues, cDCs and B cells often displayed the
363 highest HPG fluorescence intensities, while non-B lymphocytes and neutrophils generally showed
364 relatively low amounts of incorporation. HPG incorporation and metabolic profiles could not be assessed
365 in eosinophils, as these cells acquired a very high non-specific background signal after fluorescent click
366 reaction, even in the absence of HPG.

367 To visualize potential differences in immune cell metabolic profiles across tissues, glucose and
368 mitochondrial dependencies of shared immune populations were analyzed by PCA. Samples derived from
369 the same tissue clustered together, and clear group separations were observable between different
370 tissues (Figure 4B). Broadly, three clusters can be observed based on the proximity of the plotted
371 centroids, namely 1) liver and eWAT, 2) kidney and PEC, and 3) lung and spleen. The loadings of the first
372 component (PC1), explaining 38% of data variance, show that mitochondrial dependence parameters are
373 highly important for projection along this axis (Figure 4C). Indeed, monocytes, cDC1s, cDC2s, and B cells
374 exhibited variable levels of mitochondrial dependence between different tissues (Figure 4D). Compared
375 to other tissues, lung, and spleen were highly dependent on mitochondrial metabolism across all four cell
376 types (>83.0%), whereas cells derived from kidney and PEC were relatively glycolytic (52.7% - 74.1%
377 mitochondrial). Liver and eWAT did not exhibit a clear tissue-specific metabolic profile but showed similar
378 cell type-specific trends, *e.g.,* relatively mitochondrially dependent cDC1s but glycolytic cDC2s.
379 Furthermore, neutrophils, monocytes, cDC1s, cDC2s, and B cells all showed high dependence on glucose,
380 whereas $Ly6C^-$ and $Ly6C^{hi}$ non-B lymphocytes were less glucose-dependent and showed variable
381 mitochondrial dependence across tissues (Supplementary Figure 6A-C). Similar to human T cells from
382 PBMCs, several tissue-resident macrophage populations showed low levels of HPG incorporation (Figure
383 6A), leading to relatively unstable metabolic dependencies in, *e.g.,* Kupffer cells (Supplementary Figure
384 6D). Among macrophage populations, spleen macrophages appear relatively glycolytic, whereas
385 peritoneal macrophage subsets showed high mitochondrial dependence. Within PEC, a further subdivision
386 in mitochondrial metabolism could be observed between $MHCII^+$ monocyte-derived immature
387 macrophages (86.1%) and $F4/80^{hi}$ mature tissue-resident macrophages ($TIM4^-$ 97.5%, $TIM4^+$ 95.1%).

Discussion

Here, we established SCENITH-BONCAT as a valid approach for performing in-depth metabolic profiling of immune cells. We demonstrated that HPG incorporation can be used as an alternative to puromycin immunostaining as a proxy for protein synthesis. Both substrates showed that LPS/IFNγ-primed classical activation of monocyte-derived macrophages resulted in a relative increase in glycolytic capacity, while IL-4-induced alternatively activated macrophages displayed enhanced mitochondrial dependence. These results are in line with previous work in murine bone-marrow-derived macrophages (Huang et al., 2014; Van den Bossche et al., 2016), but also with a recent study on Seahorse analysis of human monocyte-derived macrophage activation (Hickman et al., 2023).

The use of HPG over puromycin as a substrate to measure protein synthesis has several advantages. Firstly, puromycin is a toxic antibiotic often used as a selection agent for eukaryotic cells. Puromycin inhibits protein translation, leading to the formation of prematurely terminated truncated polypeptides (Lacsina et al., 2012). This apparent toxicity limits the maximal substrate incorporation time and could lead to unwanted effects. HPG, on the other hand, is incorporated into full-length proteins and, therefore, relatively non-toxic (Su Hui Teo *et al.*, 2016). Secondly, compared to AHA, puromycin labeling was found to be inappropriate for accurately measuring overall protein synthesis rates during energy-starved conditions, particularly in response to glucose starvation and 2-DG treatment (Marciano et al., 2018). This could explain differences in glucose dependence measurements between both technical variants. Lastly, whereas SCENITH measurement of puromycin is reliant on a specific, non-commercially available antibody, HPG can be combined with a wide range of different azide probes covering the full spectrum of fluorescent light, providing the user with a high degree of customizability. A limitation of SCENITH-BONCAT over the original protocol is the requirement for methionine depletion before treatment, which requires specialized culture media and additional washing steps. This could be overcome by developing biorthogonal amino acids analogs that are efficiently incorporated under native culture conditions, such as a novel threonine analog that was recently described as part of a method named THRONCAT (Ignacio et al., 2023).

Application of SCENITH-BONCAT in PBMCs replicated previously published metabolic signatures of immune cell activation. For instance, stimulation with ODN2006 (CpG) enhanced HPG incorporation and glycolytic capacity in B cells, which is in line with the literature (Krieg et al., 1995) and the result of high expression of TLR9 (Hornung et al., 2002). Upon activation with LPS and other stimuli, classical monocytes reportedly switch from a mitochondrially dependent to a highly glycolytic profile (Lachmandas et al., 2016), which could be reproduced by SCENITH-BONCAT. Furthermore, $CD16^{+}/CD14^{-}$ non-classical monocytes displayed higher levels of mitochondrial dependence compared to classical $CD16^{-}/CD14^{+}$ monocytes, which is congruent with previous studies reporting increased mitochondrial activity and transcription of genes involved in mitochondrial respiration in non-classical monocytes (Schmidl et al., 2014; Zhao et al., 2010). As expected, CD4 and CD8 T cells showed strongly increased HPG incorporation in response to CD3/CD28 stimulation. Activated T cells were primarily glycolytic and glucose-dependent but also exhibited mitochondrial activity. We observed very low levels of HPG incorporation in unstimulated T cells and NK cells, indicating that these cells are metabolically quiescent under basal conditions, which is in accordance with previous research (Chapman et al., 2020; Keppel et al., 2015). As a result, minor technical variations in HPG measurements could significantly skew overall metabolic dependencies in these cells, leading to unpredictable and even negative values. This was particularly visible for oligomycin treatment, which sometimes increased HPG incorporation compared to DMSO control, possibly due to metabolic adaptation through increased glycolytic flux (Hao et al., 2010). For accurate metabolic profiling of quiescent cells, specialized SCENITH-BONCAT protocols will need to be developed, *e.g.,* which employ higher concentrations of HPG and/or longer incubation times.

Although studying circulating immune cell populations can yield valuable insights, it's important to acknowledge that they can differ significantly from their tissue-resident counterparts, which possess unique functions and metabolic profiles driven by microenvironmental imprinting. Until now, there has been a lack of suitable technologies to measure the metabolism of tissue-resident immune cells due to low cell availability and high sample complexity. By employing SCENITH-BONCAT on murine tissues, we

439 could broadly separate samples according to their residency. cDCs, B cells, and monocytes from lung and
440 spleen were generally highly mitochondrially dependent, while kidney and PEC cells were more glycolytic.
441 This potentially reflects the relative degree of tissue oxygenation, as the lungs are highly perfused while
442 the spleen serves as a reservoir for oxygen-rich erythrocytes. We observed that tissue-resident cDC1
443 cells were generally more mitochondrially dependent than their cDC2 counterparts. Consistent with this
444 finding, *in vitro*-generated cDC1s were reported to have an increased mitochondrial content and
445 membrane potential compared to cDC2s (Kratchmarov et al., 2018). Within macrophage populations,
446 kidney macrophages incorporated very low levels of HPG, in line with their reported quiescent state
447 during homeostasis (Wculek et al., 2022). Our results corroborate that peritoneal and alveolar
448 macrophages are highly mitochondrially dependent (Davies et al., 2017; Woods et al., 2020), while
449 splenic red pulp macrophages were relatively glycolytic. Wculek and colleagues observed a similar
450 ranking of murine tissue macrophages based on their relative expression of OXPHOS-related genes in
451 single-cell RNA sequencing datasets (Wculek et al., 2023). Similar to the measurements in PBMCs, low
452 levels of HPG incorporation sometimes resulted in unstable metabolic dependencies in some cell types.
453 Further optimized SCENITH-BONCAT protocols must be designed to metabolically profile tissue
454 macrophages, especially in relatively impure tissue samples such as liver and kidney.

455 In summary, SCENITH-BONCAT is a promising technique for performing in-depth metabolic profiling of
456 samples of varying complexity, spanning isolated cell types to *ex vivo* murine tissues. While tested here
457 with a focus on immune cells, SCENITH-BONCAT is not limited by cell type or tissue. Our adaptation
458 retains the benefits of the original protocol, including its independence of specialized equipment except
459 for any flow cytometer, low cell number requirement, and non-necessity for cell purification while
460 providing much-needed improvements in accessibility and customizability.

461 **Figure legends**

462

463 **Figure 1: SCENITH-BONCAT assay concept.** Created using BioRender (www.BioRender.com).

464

465 **Figure 2: Comparison of SCENITH-BONCAT with the original SCENITH protocol.** (A) Structures of
466 methionine and HPG. (B-C) Primary human macrophages (M-CSF) were treated with HPG and harvested
467 at different time points for click staining. (B) Representative flow cytometry histograms of HPG-AZ488
468 staining at 0, 0.5, 1, 2, 4, and 6 hours post-treatment. (C) HPG incorporation kinetics of macrophages
469 treated with homoharringtonine (red) or DMSO control (blue). Data are displayed as means ± SD of the
470 geometric MFI (gMFI, n=3). (D-E) Primary human macrophages (GM-CSF and M-CSF) were stimulated
471 for 24 hours with culture medium (green), LPS + IFNγ (red), or IL-4 (blue) before SCENITH analysis
472 using either HPG or puromycin (Puro) as substrates. (D) Mitochondrial dependence (%) and glycolytic
473 capacity (%) of GM-CSF macrophages. (E) Mitochondrial dependence (%) and glycolytic capacity of M-
474 CSF macrophages. Data are displayed as mean percentages ± SD (n=6). Significance was tested by
475 Two-Way ANOVA with Sidak correction for multiple testing. Individual donors are displayed by different
476 symbols. * = $p < 0.05$, ** = $p < 0.01$, *** = $p < 0.001$

477

478 **Figure 3: SCENITH-BONCAT analysis of PBMC metabolic profiles after different stimulations.**
479 (A) PBMCs isolated from healthy blood donors (n=6) were stimulated for 2 hours with Medium control
480 (green), LPS (red), ODN2006 (orange), TransAct (blue), or all stimuli combined (Mix, purple). (B)
481 Representative UMAP plot of PBMCs stained with 9-marker flow cytometry panel. (C) Fold changes of
482 HPG incorporation compared to Medium control, (D) glucose dependence (%), and (E) mitochondrial
483 dependence (%) of classical monocytes, non-classical monocytes, B cells, CD4 T cells, and CD8 T cells.
484 Significance was tested by Repeated One-Way ANOVA with Dunnett's multiple comparisons test.
485 Individual donors are displayed by different symbols. ND = Not determinable. * = $p < 0.05$, ** = $p <$
486 0.01, *** = $p < 0.001$

487

488 **Figure 4: SCENITH-BONCAT analysis of murine tissue-resident immune cell populations.** The
489 following tissues were isolated from male C57BL/6 mice (n=6) and subjected to SCENITH analysis: eWAT
490 (red), kidney (yellow), liver (green), lung (cyan), PEC (blue), spleen (pink). (A) HPG incorporation (gMFI)
491 of immune cell populations from all six tissues. (B) PCA score plot based on metabolic dependencies of
492 shared immune cell populations in all six tissues. (C) Loadings on PC1 of the PCA score plot. Measures of
493 glucose dependence are represented by red bars and mitochondrial dependence by blue bars. (D)
494 Mitochondrial dependence (%) of cDC1s, cDC2s, monocytes, and B cells from all six tissues.

References

Acin-Perez, R., Benador, I.Y., Petcherski, A., Veliova, M., Benavides, G.A., Lagarrigue, S., Caudal, A., Vergnes, L., Murphy, A.N., Karamanlidis, G., et al. (2020). A novel approach to measure mitochondrial respiration in frozen biological samples. Embo j *39*, e104073. 10.15252/embj.2019104073.

Argüello, R.J., Combes, A.J., Char, R., Gigan, J.P., Baaziz, A.I., Bousiquot, E., Camosseto, V., Samad, B., Tsui, J., Yan, P., et al. (2020). SCENITH: A Flow Cytometry-Based Method to Functionally Profile Energy Metabolism with Single-Cell Resolution. Cell metabolism *32*, 1063-1075.e1067. 10.1016/j.cmet.2020.11.007.

Aviner, R. (2020). The science of puromycin: From studies of ribosome function to applications in biotechnology. Computational and structural biotechnology journal *18*, 1074-1083. 10.1016/j.csbj.2020.04.014.

Beatty, K.E., Xie, F., Wang, Q., and Tirrell, D.A. (2005). Selective dye-labeling of newly synthesized proteins in bacterial cells. Journal of the American Chemical Society *127*, 14150-14151. 10.1021/ja054643w.

Boutens, L., Hooiveld, G.J., Dhingra, S., Cramer, R.A., Netea, M.G., and Stienstra, R. (2018). Unique metabolic activation of adipose tissue macrophages in obesity promotes inflammatory responses. Diabetologia *61*, 942-953. 10.1007/s00125-017-4526-6.

Chapman, N.M., Boothby, M.R., and Chi, H. (2020). Metabolic coordination of T cell quiescence and activation. Nature reviews. Immunology *20*, 55-70. 10.1038/s41577-019-0203-y.

Davies, L.C., Rice, C.M., Palmieri, E.M., Taylor, P.R., Kuhns, D.B., and McVicar, D.W. (2017). Peritoneal tissue-resident macrophages are metabolically poised to engage microbes using tissue-niche fuels. Nat Commun *8*, 2074. 10.1038/s41467-017-02092-0.

Dieterich, D.C., Link, A.J., Graumann, J., Tirrell, D.A., and Schuman, E.M. (2006). Selective identification of newly synthesized proteins in mammalian cells using bioorthogonal noncanonical amino acid tagging (BONCAT). Proceedings of the National Academy of Sciences of the United States of America *103*, 9482-9487. 10.1073/pnas.0601637103.

Hao, W., Chang, C.P., Tsao, C.C., and Xu, J. (2010). Oligomycin-induced bioenergetic adaptation in cancer cells with heterogeneous bioenergetic organization. The Journal of biological chemistry *285*, 12647-12654. 10.1074/jbc.M109.084194.

Hickman, E., Smyth, T., Cobos-Uribe, C., Immormino, R., Rebuli, M.E., Moran, T., Alexis, N.E., and Jaspers, I. (2023). Expanded characterization of in vitro polarized M0, M1, and M2 human monocyte-derived macrophages: Bioenergetic and secreted mediator profiles. PloS one *18*, e0279037. 10.1371/journal.pone.0279037.

Hornung, V., Rothenfusser, S., Britsch, S., Krug, A., Jahrsdörfer, B., Giese, T., Endres, S., and Hartmann, G. (2002). Quantitative expression of toll-like receptor 1-10 mRNA in cellular subsets of human peripheral blood mononuclear cells and sensitivity to CpG oligodeoxynucleotides. Journal of immunology (Baltimore, Md. : 1950) *168*, 4531-4537. 10.4049/jimmunol.168.9.4531.

Huang, S.C., Everts, B., Ivanova, Y., O'Sullivan, D., Nascimento, M., Smith, A.M., Beatty, W., Love-Gregory, L., Lam, W.Y., O'Neill, C.M., et al. (2014). Cell-intrinsic lysosomal lipolysis is essential for alternative activation of macrophages. Nature immunology *15*, 846-855. 10.1038/ni.2956.

Kaymak, I., Williams, K.S., Cantor, J.R., and Jones, R.G. (2021). Immunometabolic Interplay in the Tumor Microenvironment. Cancer cell *39*, 28-37. 10.1016/j.ccell.2020.09.004.

Keppel, M.P., Saucier, N., Mah, A.Y., Vogel, T.P., and Cooper, M.A. (2015). Activation-specific metabolic requirements for NK Cell IFN-γ production. Journal of immunology (Baltimore, Md. : 1950) *194*, 1954-1962. 10.4049/jimmunol.1402099.

Kratchmarov, R., Viragova, S., Kim, M.J., Rothman, N.J., Liu, K., Reizis, B., and Reiner, S.L. (2018). Metabolic control of cell fate bifurcations in a hematopoietic progenitor population. Immunology and cell biology *96*, 863-871. 10.1111/imcb.12040.

Krieg, A.M., Yi, A.K., Matson, S., Waldschmidt, T.J., Bishop, G.A., Teasdale, R., Koretzky, G.A., and Klinman, D.M. (1995). CpG motifs in bacterial DNA trigger direct B-cell activation. Nature *374*, 546-549. 10.1038/374546a0.

Lachmandas, E., Boutens, L., Ratter, J.M., Hijmans, A., Hooiveld, G.J., Joosten, L.A., Rodenburg, R.J., Fransen, J.A., Houtkooper, R.H., van Crevel, R., et al. (2016). Microbial stimulation of different Toll-like receptor signalling pathways induces diverse metabolic programmes in human monocytes. Nature microbiology *2*, 16246. 10.1038/nmicrobiol.2016.246.

Lacsina, J.R., Marks, O.A., Liu, X., Reid, D.W., Jagannathan, S., and Nicchitta, C.V. (2012). Premature translational termination products are rapidly degraded substrates for MHC class I presentation. PloS one *7*, e51968. 10.1371/journal.pone.0051968.

Landgraf, P., Antileo, E.R., Schuman, E.M., and Dieterich, D.C. (2015). BONCAT: metabolic labeling, click chemistry, and affinity purification of newly synthesized proteomes. Methods in molecular biology (Clifton, N.J.) *1266*, 199-215. 10.1007/978-1-4939-2272-7_14.

Le Cao, K.-A., Rohart, F., Gonzalez, I., and Dejean, S. (2021). mixOmics: Omics Data Integration Project.

Liu, Z., Gu, Y., Shin, A., Zhang, S., and Ginhoux, F. (2020). Analysis of Myeloid Cells in Mouse Tissues with Flow Cytometry. STAR protocols *1*, 100029. 10.1016/j.xpro.2020.100029.

Marciano, R., Leprivier, G., and Rotblat, B. (2018). Puromycin labeling does not allow protein synthesis to be measured in energy-starved cells. Cell death & disease *9*, 39. 10.1038/s41419-017-0056-x.

Oguma, T., Ono, T., Kajiwara, T., Sato, M., Miyahira, Y., Arino, H., Yoshihara, Y., and Tadakuma, T. (2009). CD4(+)CD8(+) thymocytes are induced to cell death by a small dose of puromycin via ER stress. Cellular immunology *260*, 21-27. 10.1016/j.cellimm.2009.07.002.

Pelgrom, L., Davis, G., O'Shoughnessy, S., Kasteren, S.V., Finlay, D., and Sinclair, L. (2022). QUAS-R: Glutamine (Q) Uptake Assay with Single cell Resolution reveals metabolic heterogeneity with immune populations. bioRxiv, 2022.2009.2029.510040. 10.1101/2022.09.29.510040.

Schmidl, C., Renner, K., Peter, K., Eder, R., Lassmann, T., Balwierz, P.J., Itoh, M., Nagao-Sato, S., Kawaji, H., Carninci, P., et al. (2014). Transcription and enhancer profiling in human monocyte subsets. Blood *123*, e90-99. 10.1182/blood-2013-02-484188.

Shen, Y., Liu, W., Zuo, J., Han, J., and Zhang, Z.C. (2021). Protocol for visualizing newly synthesized proteins in primary mouse hepatocytes. STAR protocols *2*, 100616. 10.1016/j.xpro.2021.100616.

Shirai, T., Nazarewicz, R.R., Wallis, B.B., Yanes, R.E., Watanabe, R., Hilhorst, M., Tian, L., Harrison, D.G., Giacomini, J.C., Assimes, T.L., et al. (2016). The glycolytic enzyme PKM2 bridges metabolic and inflammatory dysfunction in coronary artery disease. The Journal of experimental medicine *213*, 337-354. 10.1084/jem.20150900.

Su Hui Teo, C., Serwa, R.A., and O'Hare, P. (2016). Spatial and Temporal Resolution of Global Protein Synthesis during HSV Infection Using Bioorthogonal Precursors and Click Chemistry. PLoS pathogens *12*, e1005927. 10.1371/journal.ppat.1005927.

Van den Bossche, J., Baardman, J., Otto, N.A., van der Velden, S., Neele, A.E., van den Berg, S.M., Luque-Martin, R., Chen, H.J., Boshuizen, M.C., Ahmed, M., et al. (2016). Mitochondrial Dysfunction Prevents Repolarization of Inflammatory Macrophages. Cell reports *17*, 684-696. 10.1016/j.celrep.2016.09.008.

Van den Bossche, J., O'Neill, L.A., and Menon, D. (2017). Macrophage Immunometabolism: Where Are We (Going)? Trends Immunol *38*, 395-406. 10.1016/j.it.2017.03.001.

van den Brand, T. (2023). ggh4x: Hacks for ggplot2.

vanderZande, H.J.P., Brombacher, E.C., Lambooij, J.M., Pelgrom, L.R., Zawistowska-Deniziak, A., Patente, T.A., Heieis, G.A., Otto, F., Ozir-Fazalalikhan, A., Yazdanbakhsh, M., et al. (2023). Dendritic cell–intrinsic LKB1-AMPK/SIK signaling controls metabolic homeostasis by limiting the hepatic Th17 response during obesity. JCI Insight *8*. 10.1172/jci.insight.157948.

Verberk, S.G.S., de Goede, K.E., Gorki, F.S., van Dierendonck, X., Argüello, R.J., and Van den Bossche, J. (2022). An integrated toolbox to profile macrophage immunometabolism. Cell reports methods *2*, 100192. 10.1016/j.crmeth.2022.100192.

Warburg, O., Wind, F., and Negelein, E. (1927). THE METABOLISM OF TUMORS IN THE BODY. J Gen Physiol *8*, 519-530. 10.1085/jgp.8.6.519.

Wculek, S.K., Dunphy, G., Heras-Murillo, I., Mastrangelo, A., and Sancho, D. (2022). Metabolism of tissue macrophages in homeostasis and pathology. Cellular & molecular immunology *19*, 384-408. 10.1038/s41423-021-00791-9.

Wculek, S.K., Heras-Murillo, I., Mastrangelo, A., Mañanes, D., Galán, M., Miguel, V., Curtabbi, A., Barbas, C., Chandel, N.S., Enríquez, J.A., et al. (2023). Oxidative phosphorylation selectively orchestrates tissue macrophage homeostasis. Immunity *56*, 516-530.e519. https://doi.org/10.1016/j.immuni.2023.01.011.

Wickham, H., Chang, W., Henry, L., Pedersen, T.L., Takahashi, K., Wilke, C., Woo, K., Yutani, H., and Dunnington, D. (2023). ggplot2: Create Elegant Data Visualisations Using the Grammar of Graphics.

Wilke, C.O. (2020). cowplot: Streamlined Plot Theme and Plot Annotations for ggplot2.

Woods, P.S., Kimmig, L.M., Meliton, A.Y., Sun, K.A., Tian, Y., O'Leary, E.M., Gökalp, G.A., Hamanaka, R.B., and Mutlu, G.M. (2020). Tissue-Resident Alveolar Macrophages Do Not Rely on Glycolysis for LPS-induced Inflammation. American journal of respiratory cell and molecular biology *62*, 243-255. 10.1165/rcmb.2019-0244OC.

Zhao, C., Tan, Y.C., Wong, W.C., Sem, X., Zhang, H., Han, H., Ong, S.M., Wong, K.L., Yeap, W.H., Sze, S.K., et al. (2010). The CD14(+/low)CD16(+) monocyte subset is more susceptible to spontaneous and oxidant-induced apoptosis than the CD14(+)CD16(-) subset. Cell death & disease *1*, e95. 10.1038/cddis.2010.69.

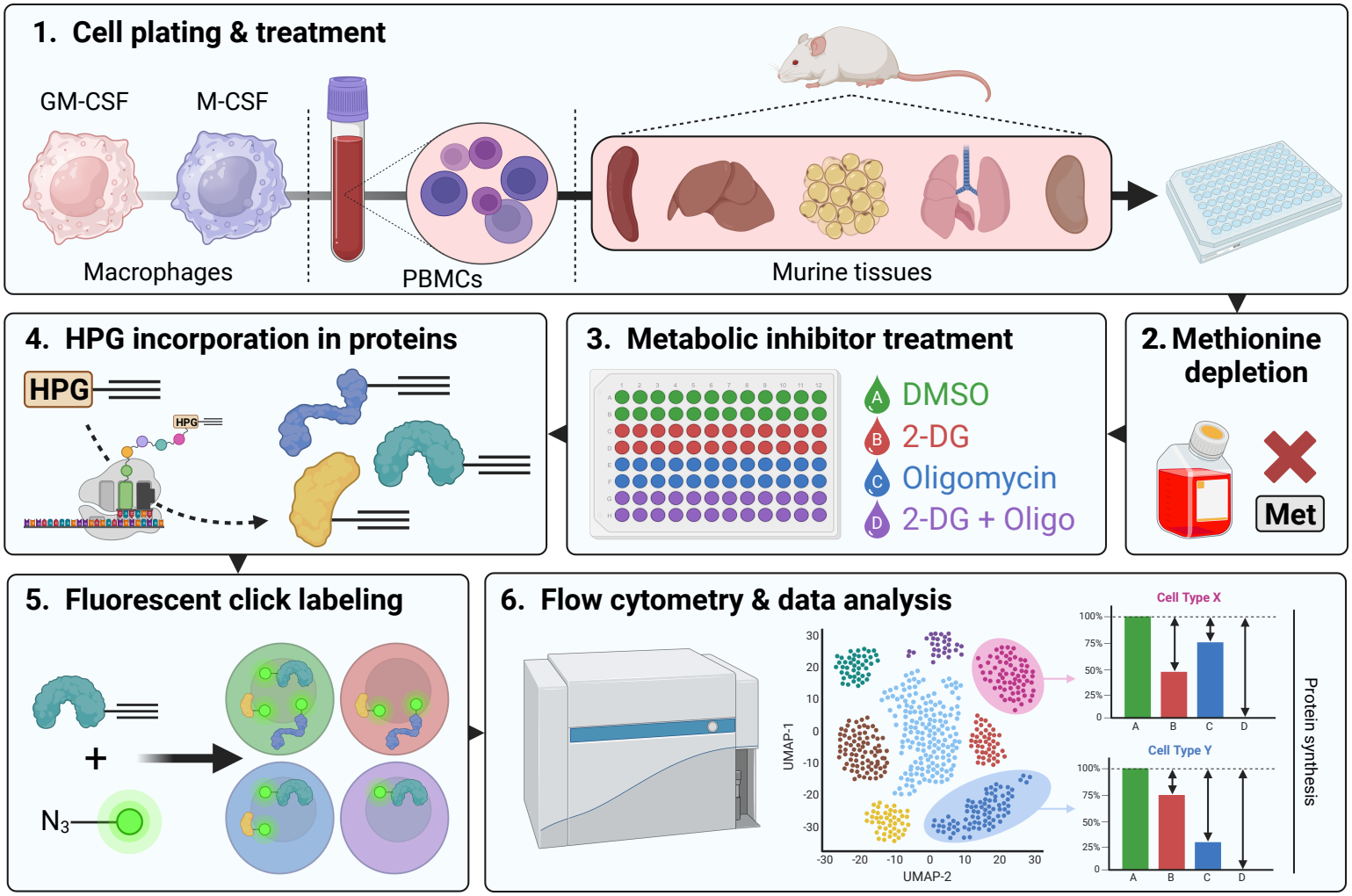
1. Cell plating & treatment
GM-CSF
M-CSF
Macrophages
PBMCs
Murine tissues
2. Methionine depletion
Met
3. Metabolic inhibitor treatment
A DMSO
B 2-DG
C Oligomycin
D 2-DG + Oligo
4. HPG incorporation in proteins
HPG
5. Fluorescent click labeling
N3
6. Flow cytometry & data analysis
UMAP-1
UMAP-2
Cell Type X
Cell Type Y
Protein synthesis

Figure 1

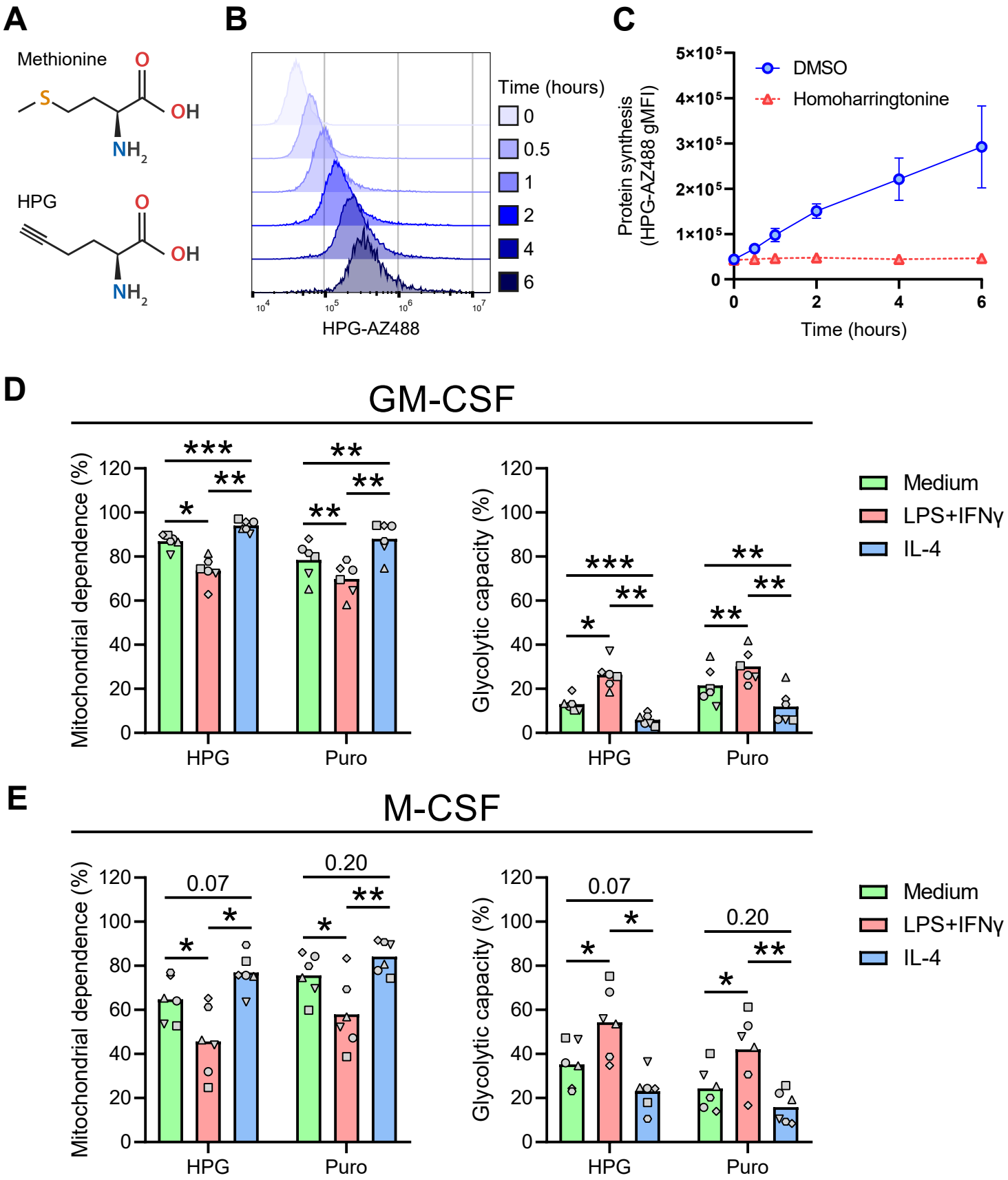
A
Methionine
HPG
B
Time (hours)
0
0.5
1
2
4
6
HPG-AZ488
C
DMSO
Homoharringtonine
Protein synthesis (HPG-AZ488 gMFI)
Time (hours)
D
GM-CSF
Mitochondrial dependence (%)
Glycolytic capacity (%)
HPG
Puro
Medium
LPS+IFNγ
IL-4
E
M-CSF
0.07
0.20

Figure 2

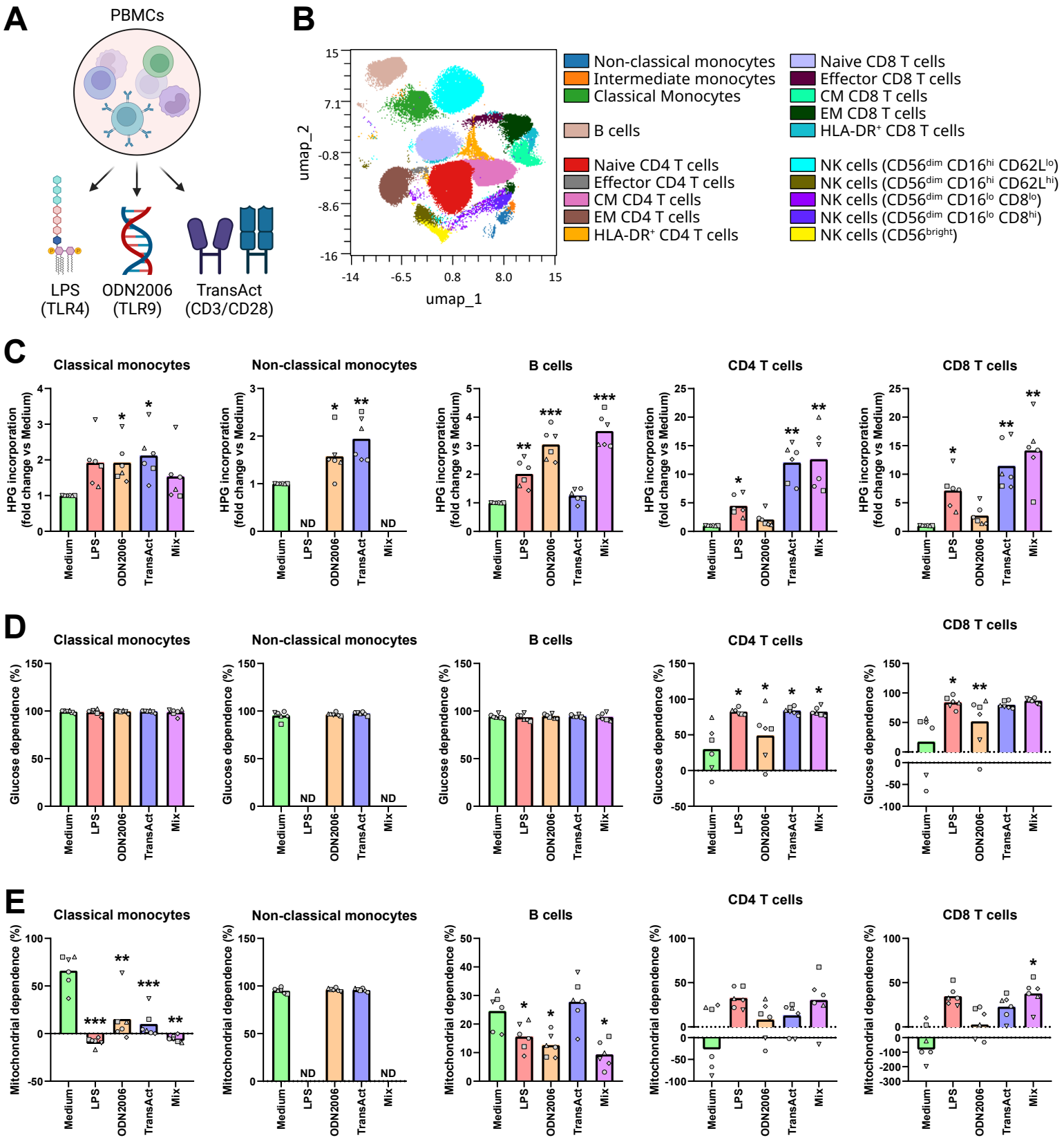
A
PBMCs
LPS (TLR4)
ODN2006 (TLR9)
TransAct (CD3/CD28)
B
umap_2
umap_1
Non-classical monocytes
Intermediate monocytes
Classical Monocytes
B cells
Naive CD4 T cells
Effector CD4 T cells
CM CD4 T cells
EM CD4 T cells
HLA-DR+ CD4 T cells
Naive CD8 T cells
Effector CD8 T cells
CM CD8 T cells
EM CD8 T cells
HLA-DR+ CD8 T cells
NK cells (CD56dim CD16hi CD62Llo)
NK cells (CD56dim CD16hi CD62Lhi)
NK cells (CD56dim CD16lo CD8lo)
NK cells (CD56dim CD16lo CD8hi)
NK cells (CD56bright)
C
Classical monocytes
Non-classical monocytes
B cells
CD4 T cells
CD8 T cells
HPG incorporation (fold change vs Medium)
Medium
LPS
ODN2006
TransAct
Mix
ND
D
Glucose dependence (%)
E
Mitochondrial dependence (%)

Figure 3

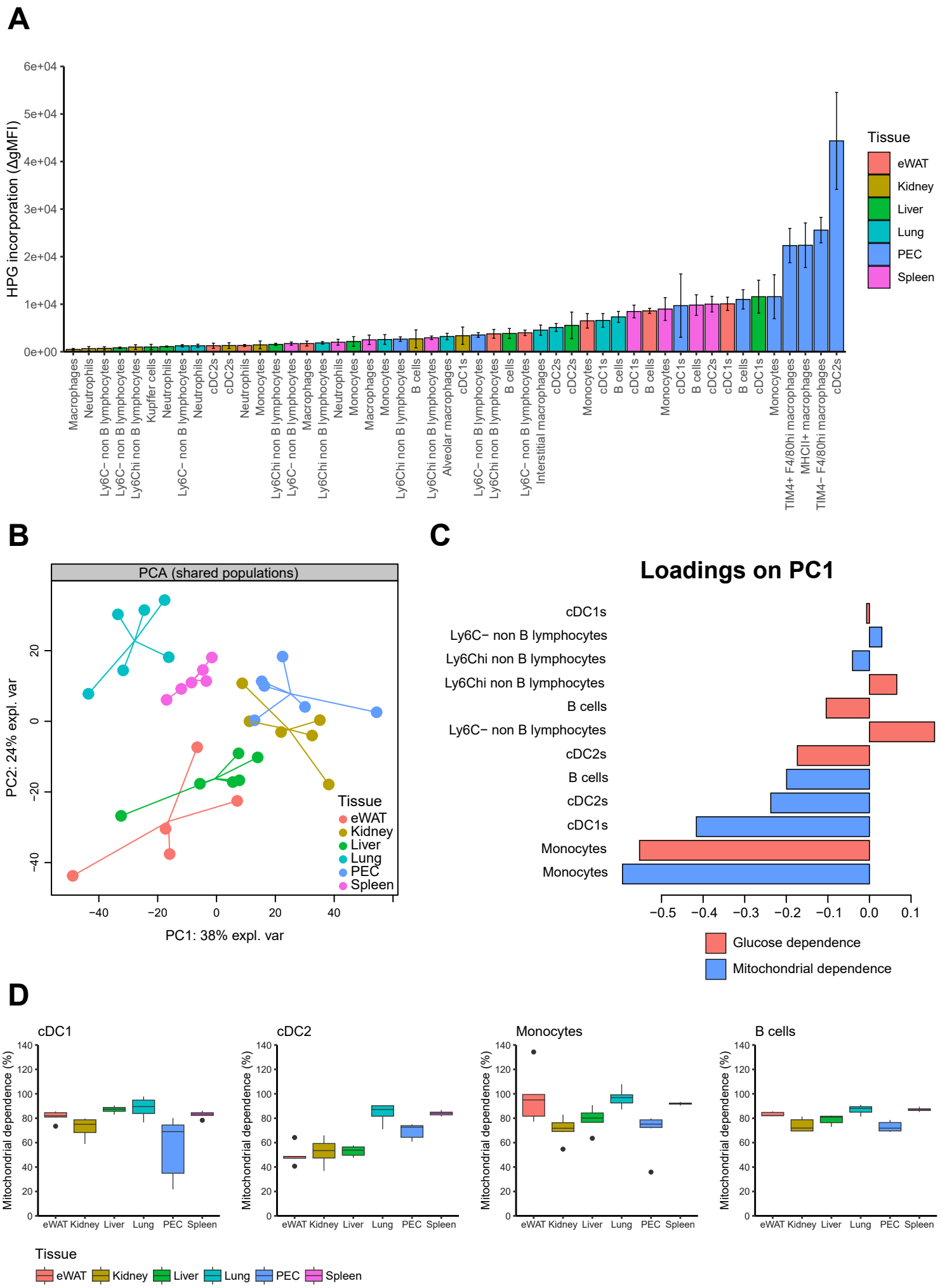
A
HPG incorporation (ΔgMFI)
6e+04
5e+04
4e+04
3e+04
2e+04
1e+04
0e+00
Macrophages
Neutrophils
Ly6C− non B lymphocytes
Ly6C− non B lymphocytes
Ly6Chi non B lymphocytes
Kupffer cells
Neutrophils
Ly6C− non B lymphocytes
Neutrophils
cDC2s
cDC2s
Neutrophils
Monocytes
Ly6Chi non B lymphocytes
Ly6C− non B lymphocytes
Macrophages
Ly6Chi non B lymphocytes
Neutrophils
Monocytes
Macrophages
Monocytes
Ly6Chi non B lymphocytes
B cells
Ly6Chi non B lymphocytes
Alveolar macrophages
cDC1s
Ly6C− non B lymphocytes
Ly6Chi non B lymphocytes
B cells
Ly6C− non B lymphocytes
Interstitial macrophages
cDC2s
cDC2s
Monocytes
cDC1s
B cells
cDC1s
B cells
Monocytes
cDC1s
B cells
cDC2s
cDC1s
B cells
cDC1s
Monocytes
TIM4+ F4/80hi macrophages
MHCII+ macrophages
TIM4− F4/80hi macrophages
cDC2s
Tissue
eWAT
Kidney
Liver
Lung
PEC
Spleen
B
PCA (shared populations)
PC2: 24% expl. var
PC1: 38% expl. var
20
0
−20
−40
−40
−20
0
20
40
Tissue
eWAT
Kidney
Liver
Lung
PEC
Spleen
C
Loadings on PC1
cDC1s
Ly6C− non B lymphocytes
Ly6Chi non B lymphocytes
Ly6Chi non B lymphocytes
B cells
Ly6C− non B lymphocytes
cDC2s
B cells
cDC2s
cDC1s
Monocytes
Monocytes
−0.5
−0.4
−0.3
−0.2
−0.1
0.0
0.1
Glucose dependence
Mitochondrial dependence
D
cDC1
cDC2
Monocytes
B cells
Mitochondrial dependence (%)
140
120
100
80
60
40
20
0
eWAT
Kidney
Liver
Lung
PEC
Spleen
Tissue
eWAT
Kidney
Liver
Lung
PEC
Spleen

Figure 4